Hindawi
International Journal of Aerospace Engineering
Volume 2023, Article ID 1111557, 16 pages
https://doi.org/10.1155/2023/1111557

Research Article

A LEO Satellite Handover Strategy Based on Graph and Multiobjective Multiagent Path Finding

Zhiyun Jiang, Wei Li, Xiangtong Wang, and Binbin Liang

School of Aeronautics and Astronautics, Sichuan University, Chengdu, Sichuan Province 610207, China

Correspondence should be addressed to Wei Li; li.wei@scu.edu.cn

Received 30 October 2022; Revised 28 December 2022; Accepted 12 January 2023; Published 30 January 2023

Academic Editor: Jinchao Chen

Low earth orbit (LEO) satellite network can provide services to users anywhere on the earth. However, the high-speed mobility of satellites leads to a dynamic environment, which brings challenges for handover and network performance optimization, especially in the scenario of multiuser using the networks meanwhile. In this paper, we exploit multiple directed graphs to model the handover process for multiuser. The nodes in a graph represent the satellites that the corresponding user may choose to access. The edges represent the possible handovers between adjacent timestamps. The path from the start node to the end node in each graph is the handover strategy of the corresponding user, and the path length is the reward that the user can get. Therefore, the handover strategy problem is transformed into a path planning problem. To minimize the average handover times, maximize the average received power, and minimize the average number of conflicts, we propose a novel handover strategy based on multiobjective multiagent path finding (MOMAPF). The simulated handover experiment on Starlink successfully derives the Pareto-optimal solution set, which corroborates the effectiveness of the proposed handover strategy. The results also show that the proposed strategy has better comprehensive performance than other strategies.

1. Introduction

In recent years, especially after SpaceX's Starlink plan is bringing into effect, the satellite-terrestrial integrated networks (STINs) have become a major research hot spot. As an important part of STIN, satellites can ignore the terrain and cover the whole earth's surface, providing communication connection for satellite communication equipment anywhere on the ground. Many studies focus on STIN's key technologies in various situations, including the association strategy between users and base stations [1, 2], gateway placement strategy [3, 4], nonorthogonal multiple access technology [5], beamforming design [6, 7], and secure transmission technology [8]. In these studies, the user terminals need to be associated with the terrestrial base stations (BSs), and the satellites are exploited to establish backhaul links with BSs to improve the network capacity (i.e., the satellites act as backhaul relays). This network structure is not suitable for user terminal communication in case of lack of ground communication facilities. In order to ensure the communication between user terminals in places without terrestrial BSs, satellites need to be exploited as BSs to establish communication links with terrestrial terminals.

Compared with geostationary orbit (GEO) and medium earth orbit (MEO), low earth orbit (LEO) has the lowest orbit altitude (≤2000 km). Therefore, LEO satellite networks have great advantages in propagation delay and energy consumption of satellite-to-ground links. It can meet the needs of real-time communication of ground user terminals. Nowadays, many institutions have explored into space and put forward plans to build their own LEO constellation. In addition to SpaceX mentioned above, Kuiper and Telesat are also included [9]. However, the lower the orbital altitude of a satellite brings, the smaller the coverage area of a single satellite and the faster the speed of the satellite. In order to achieve full coverage of the ground, a LEO system often contains thousands of satellites, forming a huge constellation. As a result, at a certain time, a user on the ground is usually covered by multiple satellites at the same time, which brings the issue of access point selection. In addition, according to 3GPP document [10], the moving speed of a LEO of altitude 600 km is 7.56 km/s, which is much higher than the rotation

speed of the earth and the moving speed of ground users. This huge speed difference between satellite and ground users causes the access points within the view range of the ground users to change rapidly. The application of terrestrial networks' strongest signal selection strategy in LEO satellite network inevitably results in frequent handover of satellite-to-ground links. Therefore, the dynamic and reasonable selection of satellite access points (i.e., handover strategy) for ground terminals needs to be studied in depth.

Many studies have focused on the access and handover strategy of LEO networks. Chowdhury et al. [11] summarized the existing satellite handover schemes comprehensively and divided them into network-layer handover and link-layer handover. The link-layer handover is then subdivided into intersatellite link (ISL) handover, spotbeam handover, and satellite handover. The network-layer handover is subdivided according to connection transfer strategies. From the perspective of methods, many handover strategies that consider various performance metrics have been proposed. Dai et al. [12] divided the throughput factor and the load balancing factor to get a new factor and then used PSO algorithm to maximize this factor to get the handover strategy. Liu et al. [13] proposed a load balanced satellite handover strategy, which also employs a power allocation optimization algorithm to improve the system capacity. Lei et al. [14] developed a handover strategy for aircraft based on user dynamic preferences. Cao et al. [15] proposed a UE-driven deep reinforcement learning- (DRL-) based method for random mobile ground terminals to maximize the average system throughput and meanwhile minimize the number of handovers in nonterrestrial networks. He et al. [16] exploited DRL to derive the handover strategy for multiuser to minimize average handover under the satellite load constraints. Considering caching capacity, remaining idle channels, and remaining service time, Leng et al. [17] proposed a DRL-based intelligent handover strategy to enhance the performance of the system. Xu et al. [18] developed a DRL-based LEO handover mechanism, which can maximize the QoE of mobile terminals by predicting the handover factor. Wang et al. [19] defined three metrics to represent four handover criteria and exploited DRL to optimize the sum of them. In addition, several studies use graph-based methods to investigate the solution of handover strategy. Wu et al. [20] exploited a bipartite graph and potential game to derive the handover strategy for multiuser to minimize the average satellite handover times and balance the load of software-defined satellite network. Feng et al. [21] also proposed a bipartite graph-based handover strategy that uses Kuhn-Munkres algorithm to match ground stations and satellites to maximize communication quality and balance the load of satellites. Wu et al. [22] modeled the satellite handover process based on graphs and then selected the shortest path algorithm to derive optimal handover strategy for a user in satellite networks. Hu et al. [23] utilized the time-expanded graph to predict handover for mobile users to avoid the handover prediction failure. Dai et al. [24] proposed a handover scheme based on dynamic space-time graph and used Floyd algorithm to obtain the optimal solution.

However, most of the above handover strategies use the weighting method to combine multiple attributes into one and then optimize it. In practice, it is intractable for decision makers to weigh the relative importance of various attributes, especially when there are three or more attributes. Besides, the dimensions of various attributes are not uniform, and the weighting method may lead to poor robustness. The emergence of Pareto-based multiobjective optimization such as NSGAII [25] and NSGAIII [26] solves these problems. In the LEO satellite networks, they can obtain a Pareto-optimal solution set, including multiple handover strategies for decision makers to choose according to the types of users. Even though there exist few handover strategies based on Pareto-based multiobjective optimization that avoid the difficulty of setting weights, the attributes they consider are relatively simple. In practice, a certain attribute of a user is often affected by other users' strategies, and this attribute does not appear in these handover strategies. Finding a handover strategy for multiuser with Pareto-based multiobjective optimization and considering the impact between users in the objective functions is a challenge.

To solve this problem, in this paper, we model the handover process of multiuser during a certain period as multiple directed graphs and obtain the handover strategy of all users through multiagent path finding (MAPF). To consider multiple attributes, we set the weight values of the edges in the multiple directed graph model as a multivariate array. Subsequently, we qualitatively analyze the impact of users choosing the same satellite during handover and define this situation as user conflict, which is represented as path conflict in the proposed multiple directed graph model. Finally, in order to avoid setting the weights, we propose a multiobjective multiagent path planning algorithm based on conflict reduction (CR-MOMAPF), which successfully combines Pareto-based multiobjective optimization with MAPF to optimize the received signal strength, handover times, and conflict times. To the best of our knowledge, this study is the first to use Pareto-based multiobjective optimization in a multiuser LEO satellite network to optimize three criterions for handover between ground users and satellites. The main contributions of this article are as follows:

(i) We model the handover process over a period for multiuser based on multiple directed graphs and formulate the optimization problem. We further propose a new parameter, called the number of conflicts between users. Users that access or hand over to the same satellite at the same time may have conflicts, which can affect some network performances. The handover optimization problem is then transformed into MOMAPF problem. We aim to minimize the average handover times, maximize the average signal reception strength, and minimize the average number of conflicts between users

(ii) The CR-MOMAPF is proposed to combine Pareto-based multiobjective with MAPF. Unlike previous graph-based handover strategies, CR-MOMAPF avoids setting the weights of each attribute to perform multiobjective optimization and considers the influence between nodes in different graphs. In addition, this algorithm can bypass the curse of

dimensionality and obtain multiple solutions for decision makers to choose

(iii) We build a huge LEO constellation as the scene and select some cities as ground users. Then, we use the proposed algorithm to find the Pareto-optimal solution set for these users in the built scene and analyze the influence of user density on Pareto front. We count the handover success rate and handover delay to show the impact of the number of user conflicts on performance. Compared with some common handover strategies, the results obtained by CR-MOMAPF have better comprehensive performance and successfully prove the effectiveness of the algorithm

The rest of this paper is organized as follows. Section 2 introduces the system model and formulates the problem. In Section 3, a handover strategy based on multiagent multiobjective path finding that can reduce the number of conflicts is proposed. Then, the simulation results are provided in Section 4. Finally, this paper is concluded in Section 5.

2. System Model and Problem Formulation

2.1. System Model. As shown in Figure 1, a LEO satellite network is composed of M satellites to serve N users in a specific time period which is divided into T timestamps. The satellites are indexed by $J = 1, \cdots, M$, and the users which are static on the ground are indexed by $i = 1, \cdots, N$. The timestamps are indexed by $t = 1, \cdots, T$. We assume that the topology and coverage areas of satellites remain unchanged during each timestamp. The set of satellites, the set of users, and the set of timestamps can be denoted by $\mathscr{M}$, $\mathscr{N}$, and $\mathscr{T}$, respectively. Significantly, in a single time stamp, a user can only select one satellite for access, and one satellite can provide services to multiple users.

2.1.1. Channel Model. Antenna gain and misalignment, transmission loss, and shadowing multipath fading are considered in this model. We assume that the antenna gains of uplink and downlink are the same. All satellites and users are equipped with parabolic antennas. The gain is given by [27]

$$G_r = G_t = \begin{cases} \eta\left(\dfrac{\pi D f}{c}\right)^2 & \text{satellites,} \\ 0 & \text{ground users,} \end{cases} \tag{1}$$

where η represents the aperture efficiency of the antenna, D is the diameter of the antenna, and c and f represent the speed of light and the transmission signal frequency, respectively.

Antenna misalignment can cause the power loss which is given by [27]

$$L = 0.00245\left(\frac{\theta D f}{c}\right), \tag{2}$$

where θ represents the angle between the antenna main reception direction and the main beam direction of the incoming signal.

Transmission loss includes many parts. In this model, we only consider free space loss, which is the main part of transmission loss. The free space loss is given by

$$\text{FSL} = 32.4 + 20 \lg d_{ij}^t + 20 \lg f, \tag{3}$$

where d_{ij}^t is the distance between satellite j and user i at t and f is the frequency of the signal.

According to the above formula and the transmitting power P_{t_j} of satellite j, the receiving power $P_{r_{ij}}$ without multipath fading and shadowing of user i is expressed as

$$P_{r_{ij}} = P_{t_j} + G_{t_j} + G_{r_i} - L - \text{FSL}. \tag{4}$$

Considering shadowing and multipath fading, we exploit the shadowed-Rician channel model in [28]. The shadowing effect is caused by obstacles between transmitter and receiver. The slowly varying local mean power Q_{ij} is generally exploited to describe the characteristics of this effect. The probability density function (PDF) of Q_{ij} is described as log-normal and given by

$$f_{Q_{ij}}(Q_{ij}) = \frac{1}{\sqrt{2\pi} s Q_{ij}} \exp\left[\frac{-\left(\ln Q_{ij} - \ln P_{r_{ij}}\right)^2}{2s^2}\right], \tag{5}$$

where s is the shadowing spread.

Given the local mean power Q_{ij}, the conditional PDF of the signal power P_{ij} in Rician fading channel is described as

$$f_{P_{ij}}(P_{ij}|Q_{ij}) = \frac{K_r + 1}{Q_{ij}} \exp\left[-K_r - \frac{(K_r + 1)P_{ij}}{Q_{ij}}\right], \\ I_0\left(\sqrt{\frac{4K_r(K_r + 1)P_{ij}}{Q_{ij}}}\right), \tag{6}$$

where $I_0(.)$ is the first kind of zeroth-order modified Bessel function. K_r is Rice factor, which represents the ratio of direct component to scattered component in the signal of the receiver. The cumulative distribution function (CDF) of P_{ij} is

$$F_{P_{ij}}(p) = \int_{-\infty}^{p}\int_{-\infty}^{+\infty} f_{P_{ij}}(P_{ij}|Q_{ij}) f_{Q_{ij}}(Q_{ij}) dQ_{ij} dP_{ij}. \tag{7}$$

The received signal power P_{ij} follows cumulative distribution $F_{p_{ij}}(p)$. So the signal strength received by user i from satellite j at time t is given by

$$p(i, j, t) = \begin{cases} F_{P_{ij}}^{-1}(y) & \text{user } i \text{ is coverd by satellite } j, \\ 0 & \text{otherwise.} \end{cases} \tag{8}$$

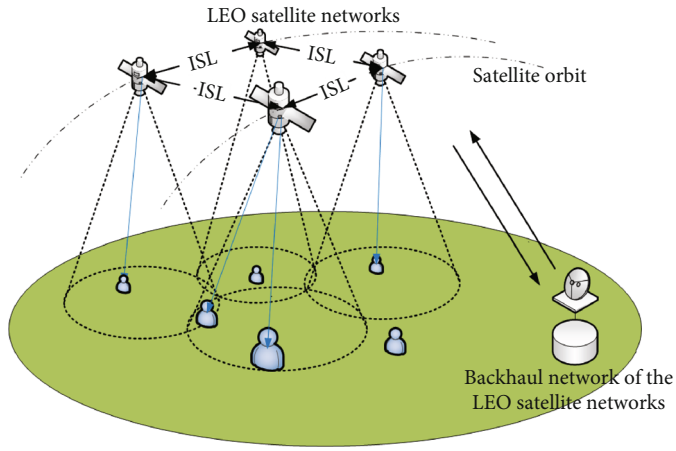

Figure 1: A LEO satellite network is composed of M LEO satellites and N ground users.

where $F^{-1}_{P_{ij}}(p)$ is the inverse cumulative distribution function of P_{ij} and y is a random variable subject to standard uniform distribution, i.e., $y \sim U[0, 1]$.

2.1.2. Multiple Directed Graph Model. As is shown in Figure 2, a directed graph is created for each user to carry out path planning, so as to obtain the handover strategy. Graphs with different colors belong to different users. The nodes in each graph represent the state of the corresponding user. Nodes $s^0_{i,\text{null}}$ and $s^{T+1}_{i,\text{null}}$ represent that the user i is not connected to any satellite and is in idle state. Within a timestamp, user i selects one of the nearest K_i satellites for access. The remaining node $s^t_{i,k}$ is the index of satellite and indicates that the user i is in the state of connecting to the kth nearest satellite $s^t_{i,k}$ within the tth timestamp. So, a satellite in different timestamps or in different graphs is regarded as different nodes in the graph model. There is an edge between every two nodes in the adjacent timestamp and no edge between any two nodes in the same timestamp. The edge indicates that the user has a state transition relationship between two timestamps, and its weight is the reward that the user can get after state transition. In this model, we can set weights representing various meanings for each edge and create an abstract agent i for user i to find the path from node $s^0_{i,\text{null}}$ (i.e., the start location) to node $s^{T+1}_{i,\text{null}}$ (i.e., the final destination). The location of the agent in each timestamp is the state of the corresponding user in the timestamp. By using the path planning algorithm, we can get the optimal path of the agent, which represents the optimal satellite selection strategy of the corresponding user during the whole time period.

Through the above directed graph model, the multiuser handover strategy problem is transformed into MOMAPF problem. Agent i makes path planning on the directed graph $G^i = (V^i, E^i)$, where V^i represents the vertex set and E^i denotes the edge set. An edge between two vertices $s^t_{i,u}, s^{t+1}_{i,v} \in V^i$ is denoted as $(s^t_{i,u}, s^{t+1}_{i,v}) \in E^i$.

In this article, three criteria need to be optimized. The handover times and received signal strength in a single user handover strategy are independent (i.e., they are not affected by the strategies of other users). The number of satellite selection conflicts is possibly affected by other users' strategies. For agent i, the weight of an edge is a binary vector, including the received signal strength $p_{s^t_{i,u}, s^{t+1}_{i,v}}$ and a binary indicator $h_{s^t_{i,u}, s^{t+1}_{i,v}}$ representing whether user i performs handover or not. They are given by

$$p_{s^t_{i,u}, s^{t+1}_{i,v}} = \begin{cases} 0 & \text{if } v = \text{null and } t = T, \\ p\left(i, s^{t+1}_{i,v}, t+1\right) & \text{otherwise,} \end{cases}$$
$$h_{s^t_{i,u}, s^{t+1}_{i,v}} = \begin{cases} 0 & \text{if } s^t_{i,u} = s^{t+1}_{i,v}, \\ 1 & \text{otherwise,} \end{cases} \tag{9}$$

where $p(i, s^{t+1}_{i,v}, t+1)$ calculates the signal strength that user i can receive at $t+1$ by selecting the satellite with index $s^{t+1}_{i,v}$ according to Equation (8). $h_{s^t_{i,u}, s^{t+1}_{i,v}} = 1$ indicates that handover occurs, while $h_{s^t_{i,u}, s^{t+1}_{i,v}} = 0$ indicates no handover.

2.1.3. User Conflict. Let π^i represent a path of agent i from node $s^0_{i,\text{null}}$ to node $s^{T+1}_{i,\text{null}}$. It is a sequence of vertices (i.e.,$\pi^i = (s^0_{i,\text{null}}, s^1_{i,k_1}, \cdots, s^T_{i,k_T}, s^{T+1}_{i,\text{null}})$). In this study, the conflict between agents is the vertex conflict, which is subdivided into two types.

We use $(i, j, s^{t_i}_{i,k_i}, s^{t_j}_{j,k_j}, \lambda)$ to denote a conflict of type of λ between users $i, j \in \mathcal{N}$. $\lambda = 1$ indicates that two users i, j access or hand over to the same satellite at the same time. $\lambda = 2$ indicates that user i hand overs to the satellite already serving another user j. The λ will affect the user's avoidance strategy when resolving the conflict in the following algorithm. We use $\varphi_{i,j}(t)$ to count the number of conflicts caused by user i to user j at t timestamp:

$$\varphi_{i,j}(t) = \begin{cases} 1 & \left(\text{t} = 1, \pi^{\text{i}}[t] = \pi^{\text{j}}[t]\right) \text{ or } \left(\text{t} \neq 1, \pi^{\text{i}}[t] = \pi^{\text{j}}[t], \pi^{\text{j}}[t-1] \neq \pi^{\text{j}}[t]\right), \\ 0 & \text{otherwise.} \end{cases} \tag{10}$$

$\varphi_{i,j}(t) = 1$ indicates that the two users i, j have a conflict at time t and $\varphi_{i,j}(t) = 0$ otherwise.

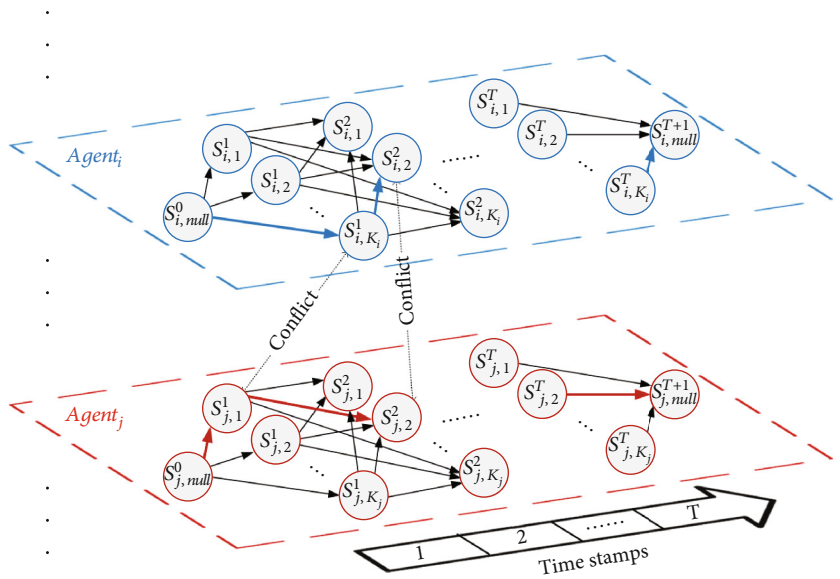

FIGURE 2: The multiple directed graph model of agents and an example of conflicts between agent i and agent j.

Then, we use matrix A to record the number of conflicts between all agents, and its element $a_{i,j}$ represents the total number of conflicts caused by agent i to agent j. $a_{i,j}$ is given by

$$a_{i,j} = \begin{cases} 0 & \text{if } i = j, \\ \sum_{t=1}^{T} \varphi_{i,j}(t) & \text{otherwise.} \end{cases} \tag{11}$$

2.1.4. User Conflict Analysis. Conflicting users compete for certain resources on the satellite they choose, thus affecting some aspects of their network performance. For multiple access protocol in LEO satellite networks, users compete for channel resources and bandwidth resources.

For example, according to results in [29], in the *orthogonal frequency division multiplexing-* (OFDM-) based LEO satellite communication system, with the increase of the number of users, the average uplink rate and downlink rate decrease. In addition, according to [30], we know that users who access the same satellite at the same time share the computing resources of the satellite equally. Therefore, with the increase of users accessing the satellite, the computing resources allocated to each user are reduced, which further affects the authentication delay, handover delay, etc. In addition, reducing the number of users accessing the same satellite can also reduce the load of the satellite.

Based on the above analysis, we can conclude that reducing the number of users switching to satellite j at the same time (i.e., called conflict in this paper) allows these users to be allocated more network resources, thus improving network performance. Therefore, we take minimizing the number of conflicts as one of the optimization objectives of this paper.

2.1.5. Handover Delay. The handover delay mainly includes the signal propagation delay in the handover procedure and the time delay for the satellite to verify the user's identity. The former is related to the distance between the satellite and the user, and the latter is related to the onboard processing capacity of the satellite. According to [30], the available computing resource for user i allocated by satellite j is

$$\alpha_{ij}(t) = \frac{F_j}{N_j(t)}, \tag{12}$$

where F_j is a constant representing the computing resources provided by each satellite j. $N_j(t)$ is the number of users accessing satellite j at t. The authentication delay for satellite j to authenticate the identity of user i is [30]

$$S_{ij}(t) = \frac{B}{a_{ij}(t)}, \tag{13}$$

where B denotes the amount of calculation required for each user in the handover procedure. We assume four signaling exchanges between the user and the target satellite after the source satellite notifies the user of the handover. Therefore, the handover delay for user i to handover to satellite j at t is

$$\mathrm{HT}_{ij}^{t} = S_{ij}(t) + 4 \cdot \frac{d_{ij}^{t}}{c}. \tag{14}$$

2.1.6. Handover Success or Failure. The user's selection of satellite at a handover directly affects the success of the handover. According to [19], the coverage relationship of the satellite to the user, the communication quality of the link between the satellite and the user, and the load of the satellite all determine whether the handover is successful for the user. We use the value of $r_{i,j}(t)$ to indicate whether the handover from user i to satellite j is successful at t. $r_{i,j}($

t) is given by [19]

$$r_{i,j}(t) = \begin{cases} 0, & \text{user } i \text{ is not covered by satellite } j \text{ or } \mathrm{CNR}_{i,j}^{t} \\ & < \mathrm{CNR}_{\min} \text{ or } N_j(t) > N_j^{\max}, \\ 1, & \text{otherwise}, \end{cases} \tag{15}$$

where $N_j^{\max}$ is the maximum channel number of satellite j. $\mathrm{CNR}_{i,j}^{t}$ is the carrier to noise ratio of the link between user i and satellite j at t. $\mathrm{CNR}_{\min}$ is the carrier to noise ratio threshold. When $\mathrm{CNR}_{i,j}^{t}$ is less than $\mathrm{CNR}_{\min}$, it indicates that the link quality is poor. $\mathrm{CNR}_{i,j}^{t}$ is given by [19]

$$\mathrm{CNR}_{i,j}^{t} = \frac{p(i,j,t)}{k_B B_d T_{\mathrm{tem}}}, \tag{16}$$

where k_B is the Boltzmann's constant (1.38×10^{-23} W/(Hz•K)). B_d is the bandwidth of shared spectrum. T_{tem} is the thermodynamic temperature of the receiver.

2.2. Problem Formulation. The cost vector c^i of a single user path π^i is defined as a binary vector including handover times and signal strength, i.e., $c^i = (f_1^i, f_2^i)$. It is the cost vector of *Individualsearch* procedure in the following algorithm. Let $\pi_k = (\pi_k^1, \pi_k^2, \cdots, \pi_k^N)$ represent a joint path for all the users, which is also called a solution. The size of a solution is $N \times T$. Take the average number of conflicts contained in this solution as another cost element. The cost vector of a solution is defined as $c_k = (\bar{f}_1, \bar{f}_2, \bar{f}_3)$. Therefore, this three-objective optimization can be formulated by

$$\begin{aligned} \max \bar{f}_1 &= \frac{1}{N}\sum_{i=1}^{N} f_1^i = \frac{1}{N}\sum_{i=1}^{N}\sum_{\left(s_{i,u}^t, s_{i,v}^{t+1}\right)\in E^i} x_{s_{i,u}^t, s_{i,v}^{t+1}} p_{s_{i,u}^t, s_{i,v}^{t+1}} \\ \min \bar{f}_2 &= \frac{1}{N}\sum_{i=1}^{N} f_2^i = \frac{1}{N}\sum_{i=1}^{N}\sum_{\left(s_{i,u}^t, s_{i,v}^{t+1}\right)\in E^i} x_{s_{i,u}^t, s_{i,v}^{t+1}} h_{s_{i,u}^t, s_{i,v}^{t+1}} \\ \min \bar{f}_3 &= \frac{1}{N}\sum_{i=1}^{N}\sum_{j=1}^{N} a_{i,j} \\ \text{s.t.} x_{s_{i,u}^t, s_{i,v}^{t+1}} &\in \{0,1\}, \quad \forall i \in \mathcal{N}, \forall \left(s_{i,u}^t, s_{i,v}^{t+1}\right) \in E^i, \end{aligned} \tag{17}$$

where $x_{s_{i,u}^t, s_{i,v}^{t+1}}$ is a binary indicator representing whether agent i passes through the edge $(s_{i,u}^t, s_{i,v}^{t+1})$ or not, i.e.,$x_{s_{i,u}^t, s_{i,v}^{t+1}} = 1$ if the agent i passes through edge $(s_{i,u}^t, s_{i,v}^{t+1})$ and $x_{s_{i,u}^t, s_{i,v}^{t+1}} = 0$ otherwise. Given the paths of all agents, we can get the handover success rate of the corresponding users under the handover strategies, which is the ratio of the successful handover times of these users to the total handover times [31].

$$\mathrm{hs} = \frac{\sum_{i=1}^{N}\sum_{\left(s_{i,u}^t, s_{i,v}^{t+1}\right)\in E_i} x_{s_{i,u}^t, s_{i,v}^{t+1}} h_{s_{i,u}^t, s_{i,v}^{t+1}} r_{i, s_{i,v}^{t+1}}(t+1)}{\sum_{i=1}^{N}\sum_{\left(s_{i,u}^t, s_{i,v}^{t+1}\right)\in E_i} x_{s_{i,u}^t, s_{i,v}^{t+1}} h_{s_{i,u}^t, s_{i,v}^{t+1}}}. \tag{18}$$

Subsequently, we use the dominance relationship between the vectors to compare the cost vectors of any two solutions and finally get the Pareto-optimal solution set.

3. Proposed MOMAPF-Based Handover Strategy for Multiuser

MAPF has been deeply studied in the field of robots and UAVs, and many algorithms have been developed, including A∗-based approaches [32] and Conflict-Based Search (CBS) [33]. However, there are few studies on the MOMAPF problem of NP-hard [34]. The studies in [34, 35], and [36] are based on a grid map scenario, and all the agents are on the same map. In addition, these studies enforce that conflict cannot occur, which is inconsistent with our goal of reducing the number of conflicts. Here, we propose CR-MOMAPF for multiagent multiobjective optimization in multiple directed graphs to obtain multiuser handover strategy in LEO satellite networks.

The proposed CR-MOMAPF algorithm is an extension of CBS, which has two key points: two level search and conflict split. For the low level in two level search, each agent carries out path finding without considering other agents. Then, the high level in two level search solves the conflict between the paths obtained by the low level of multiagent. The specific approach to solve the conflict is to adopt conflict split, which splits the conflict into multiple constraints and then gives the constraints to the corresponding agents. The generation process of CR-MOMAPF solutions is visualized in Figure 3. The purpose of the initialization stage is to generate the initial root nodes (i.e., the blue nodes). In the search stage, for the root nodes that have not been abandoned, as long as conflicts are found, child nodes will be generated. Through iteration, nodes with better and better cost vectors are obtained. The goal of this stage is to find nodes with excellent cost vectors, and the solutions represented by these nodes are the final output of the algorithm. The specific process of each stage of CR-MOMAPF is described in Algorithm 1.

3.1. Initialization Stage. In the initialization stage, according to the Two-Line Orbital Element (TLE) information of the satellite constellation, each user calculates the distance of the satellite within multiple timestamps. To implement the path planning algorithm, a directed graph G^i is constructed for each user i, and various weights and meanings are given to the edges and nodes in the graph according to the distance file and the previously mentioned channel model. Then, P (the Pareto-optimal solution set), P_1 (the Pareto-front), and *OPEN* (node set to be searched) are set as empty sets. Based on the graph G^i, aiming at minimizing f_1^i and maximizing f_2^i, each user i executes *Individualsearch*

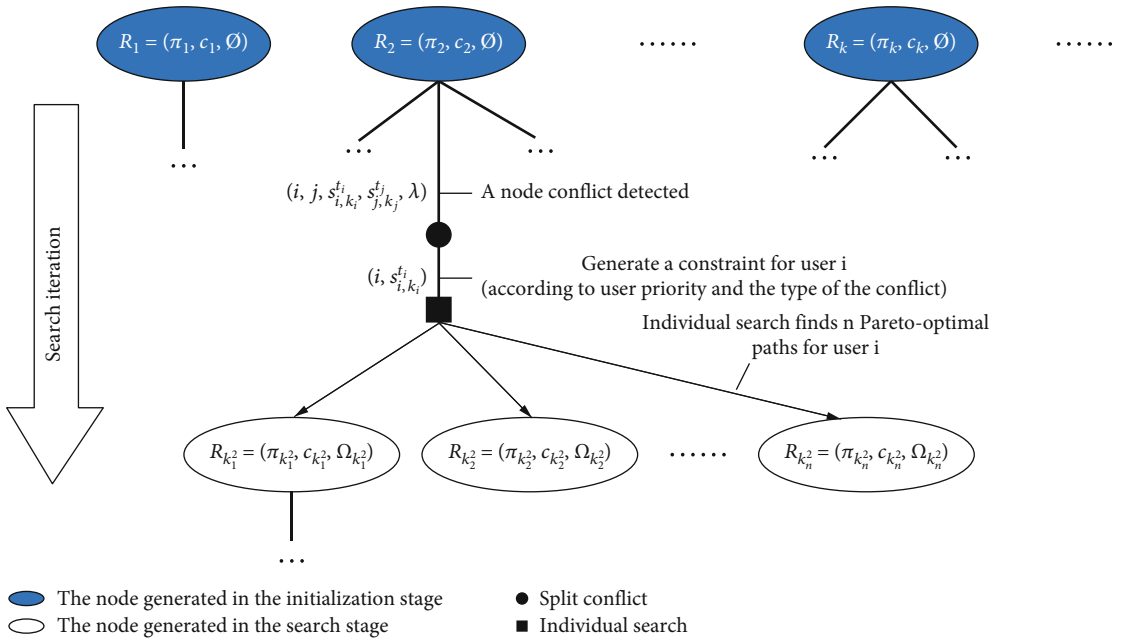

Figure 3: Search process of CR-MOMAPF.

procedure (i.e., multiobjective single-agent path finding algorithm) to find individual Pareto-optimal solution set O_i without constraint.

3.2. Search Stage. In this stage, a set of joint paths Π is generated by taking the combination of O_i, $\forall i \in \mathcal{N}$, i.e., $\Pi = \{\pi_k | \pi_k = (\pi_k^1, \pi_k^2, \cdots, \pi_k^N), \pi_k^i \in O_i, \forall i \in \mathcal{N}\}$. Then, for each joint path $\pi_k \in \Pi$, c_k, π_k, and the constraints (empty set) are combined to form a search node $R_k(\pi_k, c_k, \Omega_k)$ and added to *OPEN*.

For each search iteration in CR-MOMAPF (lines 14-42), a search node $R_k(\pi_k, c_k, \Omega_k)$ is popped from *OPEN*. Then, the *Check* procedure is exploited to determine whether the node R_k is worth continuing the search. If there is no vector dominating c_k in P_1 (i.e., $Check(R_k) = False$), we think node R_k is worth continuing to search, otherwise the node is discarded. With the *Update* procedure, those cost vectors dominated by c_k in P_1 and their corresponding strategies are removed from P_1 and P, respectively. Then, π_k and c_k are added into P and P_1, respectively. The procedure *Update* is necessary due to the fact that it can ensure that the vectors in P_1 are Pareto-optimal in the whole search iteration progress. As a result, P_1 is guaranteed to be the excellent Pareto-optimal front when the algorithm terminates.

If there is no conflict in π_k, then π_k is a Pareto-optimal solution because it has the best performance in terms of $\bar{f}_3$ and no other vector can dominate it. If a conflict $(i, j, s^{t_i}_{i,k_i}, s^{t_j}_{j,k_j}, \lambda)$ is detected in π_k, we adopt the split conflict approach in CBS to resolve the detected conflict. However, different from CBS, here, we split a detected conflict to generate only one constraint $(i, s^{t_i}_{i,k_i})$ according the priority of users and the type of this conflict. The priority can determine which agent to change the node selection in case of a path conflict (i.e., determine which user's constraint to generate). It can be set manually by the importance of the user or other factors. The constraint $(i, s^{t_i}_{i,k_i})$ indicates that the path of agent i cannot contain node $s^{t_i}_{i,k_i}$. There may be multiple conflicts in π_k, and a new set of constraints Ω is generated.

For each constraint $\omega^i \in \Omega$ (lines 26–40), a new set of constraints Ω_l is generated by combining ω^i with Ω_k. Then, agent i executes the *Individualsearch* procedure to get individual Pareto-optimal solution set O_i^* under the restriction of constraints Ω_l^i of user i in Ω_l. Hereafter, for each o_i^*, we get a new solution π_l by copying π_k and then replace π_l^i in π_l with o_i^*. If there is no vector dominating the cost vector c_l of π_l in P_1, a new search node $R_l(\pi_l, c_l, \Omega_l)$ is created and added into the *OPEN*. This system stage continues until there is no search node in the *OPEN*.

4. Simulation and Result

4.1. Scene Construction. To evaluate the effectiveness of the proposed algorithm, we first build a scene including a LEO satellite constellation and some ground users. For the satellite constellation, we build a typical LEO satellite constellation, Starlink, according to the constellation data in [37]. The parameters of this Starlink constellation are provided in Table 1, and the visualization is shown in Figure 4.

Due to the huge difference in the mobile speed between LEO satellites and ground users, we assume that the ground users are stationary and select some cities to represent the ground users. Their position parameters, number of visible satellites, and priority are provided in Tables 2 and 3. Num represents the average number of satellites simultaneously covering the ground user in the whole constellation period. In the first type of conflict $(i, j, s^{t_i}_{i,k_i}, s^{t_j}_{j,k_j}, 1)$ between two

Input: a distance file of all users
Output: P, P_1
Initialization stage:
Build a set of directed graphs for all users from the distance file
$P \longleftarrow \varnothing$, $P_1 \longleftarrow \varnothing$, $OPEN \longleftarrow \varnothing$
for each user i in $\mathcal{N}$ **do**
  $O_i \longleftarrow Individualsearch(i, \varnothing)$
end for
Generate a set of joint paths Π
for all $\pi_k \in \Pi$ **do**
  $\Omega_k \longleftarrow \varnothing$
  $c_k \longleftarrow$ compute path cost of π_k
  Create $R_k(\pi_k, c_k, \Omega_k)$ and add it to $OPEN$
end for
Search stage:
while $OPEN$ not empty **do**
  $R_k(\pi_k, c_k, \Omega_k) \longleftarrow OPEN.pop(.)$
  if $Check(R_k) = False$ **then**
    $Update(P)$, $Update(P_1)$
    Add π_k to P and c_k to P_1
  else
    Continue
  end if
  if no conflict detected in π_k **then**
    Continue
  else
    $\Omega \longleftarrow$ split detected conflict
    for each $\omega^i \in \Omega$ **do**
      $\Omega_l = \Omega_k \cup \omega^i$
      $O_i^* \longleftarrow Individualsearch(i, \Omega_l^i)$
      for all $o_i^* \in O_i^*$ **do**
        $\pi_l \longleftarrow \pi_k$
        Replace π_l^i in π_l with o_i^*
        $c_l \longleftarrow$ compute path cost of π_l
        Create $R_l(\pi_l, c_l, \Omega_l)$
        if $Check(R_l) = False$ **then**
          Add R_l to $OPEN$
        else
          Continue
        end if
      end for
    end for
  end if
end while
return P, P_1

Algorithm 1: Pseudocode for CR-MOMAPF-based handover strategy.

Table 1: Scene parameters.

Parameters	Values
Altitude	550 km
Orbital planes	24
Satellites per plane	66
Inclination	53°
Satellite half angle of view	44.85°
Minimum communication elevation	40°

users, the user with lower priority needs to change the policy to reduce the number of conflicts. In the second type of conflict $(i, j, s_{i,k_i}^{t_i}, s_{j,k_j}^{t_j}, 2)$ between two users, user i needs to change the policy. In this paper, we take NSGAIII [26] as the algorithm of the *Individualsearch* procedure and priority-based coding [39] as the coding method of NSGAIII. Other parameters used to calculate the objective function are shown in Table 4.

4.2. Individualsearch Procedure Performance Analysis. Here, we analyze the factors affecting f_1^i and f_2^i calculated by the

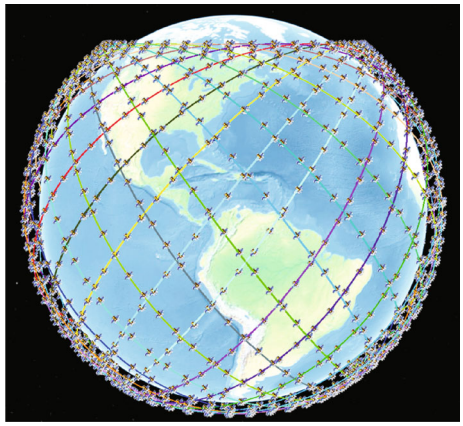

Figure 4: Huge LEO satellite constellation, Starlink, which is drawn by cesium [38].

Table 2: The parameters of cities.

Scenario	City	Lat/Lon (°)	Num	Priority
1 (sparse)	Guangzhou	29.13/113.26	2.97	0
	Tokyo	35.69/139.69	3.86	1
	Sydney	-33.87/151.21	3.67	2
	Xi'an	34.29/108.94	3.71	3
	Islamabad	33.70/73.06	3.65	4
2 (general)	Chongqing	29.56/106.55	3.32	0
	Chengdu	30.67/104.07	3.39	1
	Xi'an	34.29/108.94	3.71	2
	Changsha	28.23/112.94	3.14	3
	Wuhan	30.58/114.27	3.40	4
3 (dense)	Shanghai	31.22/121.46	3.43	0
	Nanjing	32.05/118.79	3.51	1
	Wuxi	31.54/120.30	3.47	2
	Hangzhou	30.29/120.16	3.37	3
	Hefei	31.86/117.28	3.49	4

Individualsearch procedure. Given a specific number of users in the scenario, we use three levels to measure the density of these users. The first level is sparse, which means that no satellite can cover multiple users at the same time. The second level is general, which means that a single satellite can cover multiple users at the same time, but not all users. The third level is dense, which indicates that a single satellite can cover all ground users. We construct three scenarios with different user density levels, and the initial Pareto fronts of users obtained by *Individualsearch*$(i, \varnothing)$ procedure are shown in Figure 5. The user's location (latitude, longitude) is used to represent the user, and different colored Pareto fronts belong to different users. The bidirectional Hausdorff distance values [40] between any two of the three Pareto fronts of the blue user (i.e., user with location (30, 104)) in the three scenarios are 0. So, these three Pareto-front are exactly the same. This indicates that user density does not affect handover times and received signal power of a single user. In addition to the constraints of the paths of users (i.e., the parameters of *Individualsearch*(.) procedure), f_1^i and f_2^i are only affected by their own location (i.e., longitude and latitude).

Table 3: The parameters of cities.

City	Lat/Lon (°)	Num	Priority
Chongqing	29.56/106.55	3.32	0
Chengdu	30.67/104.07	3.39	1
Xi'an	34.29/108.94	3.71	2
Changsha	28.23/112.94	3.14	3
Wuhan	30.58/114.27	3.40	4
Shanghai	31.22/121.46	3.43	5
Nanchang	28.68/115.88	3.25	6
Zhengzhou	34.76/113.65	3.75	7
Hangzhou	30.29/120.16	3.37	8
Hefei	31.86/117.28	3.49	9
Lanzhou	36.06/103.79	3.91	10
Kunming	25.04/102.72	3.06	11
Taiyuan	37.86/112.55	4.16	12
Guiyang	26.58/106.72	3.16	13
Beijing	39.91/116.40	4.48	14

Table 4: The parameters of simulation.

Parameters	Values
Transmission signal power of each satellite	50 dBw
Carrier frequency	6 GHz
s of shadowing	4 dB
K_r for Rician fading	10
T	50
Duration of each timestamp	10 s
Population size of *Individualsearch*	1000
Evolution algebra of *Individualsearch*	1000
Cross rate of *Individualsearch*	0.9
Variation rate of *Individualsearch*	0.2
Parameters in Equation (1)	$\eta = 0.55$, $D = 3$ m
B_d	1 MHz
T_{tem}	290 K
CNR_{min}	4 dB
$N_j^{\max}$	3
F_j	2200 MIPS [30]
B	6.6 M [30]

4.3. CR-MOMAPF with Different Density Levels of Users. We construct three scenarios with 5 ground users each based on the user density levels in Section 4.2. The parameters of users are shown in Table 3. Depending on the Num parameter

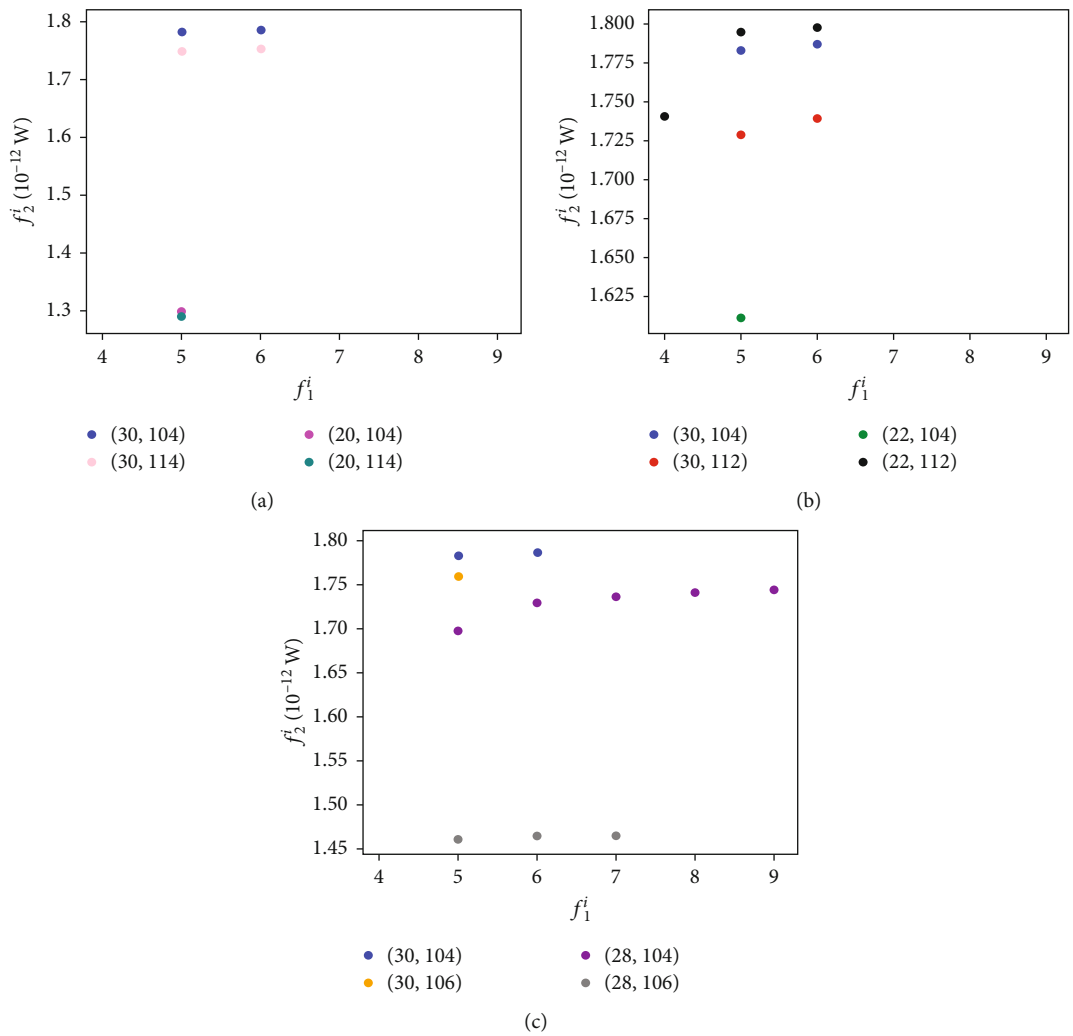

Figure 5: The initial Pareto front of users with different density levels of users: (a) sparse; (b) general; (c) dense.

value of each user in Table 2, we set the K_i of user i to 3 or 4. The Pareto front of the proposed algorithm with different density levels of users is shown in Figure 6. Eight solutions in each scenario are randomly selected from their Pareto-optimal solution sets and then presented in Table 5. The corresponding numbers of Pareto-optimal solutions obtained in the three scenarios are 19, 56, and 99, respectively. So, the number of Pareto-optimal solutions increases when the density level grows. In addition, through comparison, we can observe that the average number of conflicts also increases when the density level grows. In other words, the Pareto front becomes higher when the density level grows. Specifically, when the distance between any two users in the scenario is greater than the coverage diameter of a single satellite, there can be no conflict between users. In this case, the problem in this paper becomes a two-objective optimization problem. As described in Section 4.2, f_1^i and f_2^i are only affected by the user's location. So, for average handover times and average signal reception strength, their own distribution differences in different scenarios are caused by the differences in the location of users and the constraints generated by conflict split.

4.4. Unilateral Performance with Different Strategies. Here, we compare the performance of the proposed CR-MOMAPF with the following handover strategies:

(1) RSS-based strategy [41]: each ground user accesses the satellite that provides the strongest signal strength within each timestamp

(2) Minimum handover time- (MHT-) based handover strategy: based on the graph in [22], we set the weight of the edge as handover times and adopt Dijkstra's shortest path algorithm to realize this handover strategy

(3) Minimum conflict time- (MCT-) based handover strategy: different ground users try to select different satellites for access within each timestamp. Based on

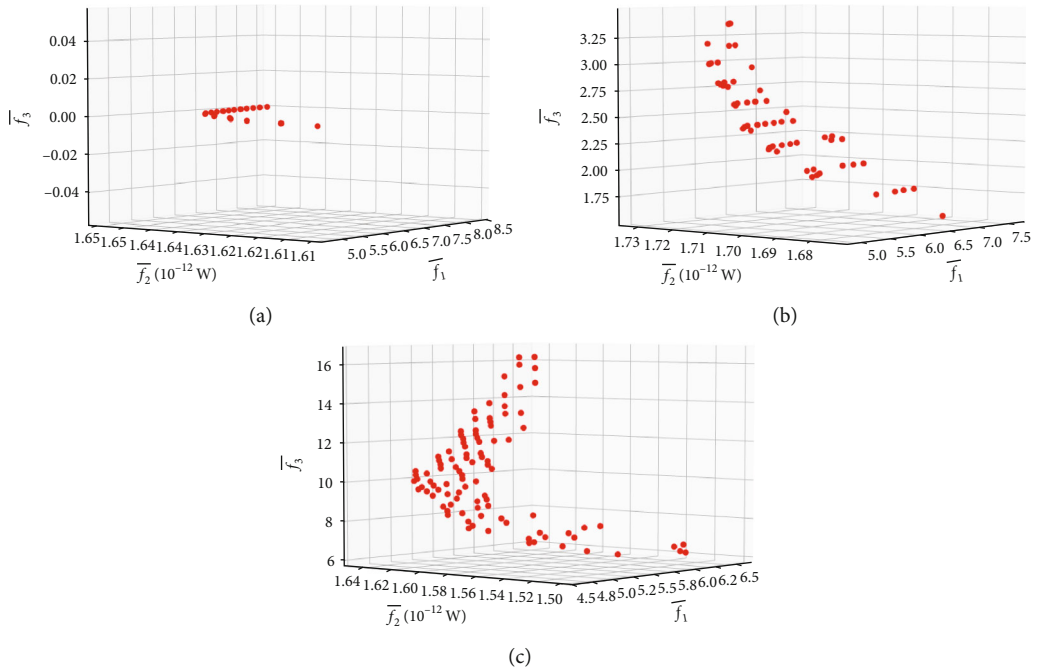

Figure 6: The Pareto front with different density levels of users: (a) Scenario 1 (sparse); (b)Scenario 2 (general); (c) Scenario 3 (dense).

Table 5: Some results to show the trade-off among different objectives.

(a)

Obj	Scenario 1 ($N = 5$, sparse)								Scenario 2 ($N = 5$, general)							
	x_1	x_2	x_3	x_4	x_5	x_6	x_7	x_8	x_1	x_2	x_3	x_4	x_5	x_6	x_7	x_8
$\overline{f_1}$	8.4	4.8*	6.8	7.6	5.0	6.4	5.2	7.2	6.4	5.0*	6.6	5.6	6.2	6.6	5.4	7.2
$\overline{f_2}$	1.650*	1.612	1.647	1.649	1.620	1.646	1.628	1.648	1.730*	1.679	1.674	1.722	1.686	1.727	1.707	1.706
$\overline{f_3}$	0.0	0.0	0.0*	0.0	0.0	0.0	0.0	0.0	2.8	2.4	1.6*	3.0	1.8	2.6	2.4	2.0

(b)

Obj	Scenario 3 ($N = 5$, dense)								Scenario 4 ($N = 10$, general)							
	x_1	x_2	x_3	x_4	x_5	x_6	x_7	x_8	x_1	x_2	x_3	x_4	x_5	x_6	x_7	x_8
$\overline{f_1}$	6.6	4.6*	6.2	5.2	5.6	6.4	5.8	5.2	7.1	4.8*	6.9	6.3	6.2	5.8	6.7	6.4
$\overline{f_2}$	1.643*	1.571	1.512	1.630	1.634	1.641	1.637	1.554	1.695*	1.637	1.585	1.691	1.693	1.688	1.694	1.694
$\overline{f_3}$	16.2	8.0	6.4*	11.0	11.2	13.2	11.8	7.4	7.1	4.8	2.7*	4.9	5.3	5.0	5.8	5.8

(c)

Obj	Scenario 5 ($N = 15$, general)											
	x_1	x_2	x_3	x_4	x_5	x_6	x_7	x_8	Weighted-based	MHT-based	MCT-based	RSS-based
$\overline{f_1}$	6.9	4.9*	5.7	6.0	5.6	4.9	6.4	5.5	15.6	3.0	35.8	7.3
$\overline{f_2}$	1.681*	1.618	1.623	1.666	1.633	1.629	1.679	1.638	1.270	1.388	1.165	1.690
$\overline{f_3}$	4.9	3.5	3.1*	3.9	3.3	3.8	4.8	3.3	3.3	3.8	0.9	6.8

∗ represents that this value is the optimal value of the objective function in the Pareto-optimal solution set.

geatpy [42], we adopt SOGA (single-objective genetic algorithm) to realize the handover strategy

(4) Weighted-based handover strategy [43]: the weight of the received signal strength, the handover times, and the conflict times are set as by $w_1 = 1/3$, $w_2 = 1/3$, and $w_3 = 1/3$. Then, we exploit single-objective optimization to get the optimal solution based on geatpy

In this simulation, in order to make the results more obvious, we set more users in the scene. We take 15 cities in Table 3 as ground users. The Pareto front obtained by CR-MOMAPF is shown in Figure 7. The Pareto-optimal solution set contains 427 solutions. We randomly select a solution from it and show the performance difference between this solution and the solutions of other strategies in Figure 8. From Figure 8(a), we can observe that users can receive the strongest signal strength under the RSS-based strategy, while the signal strength that users can receive under CR-MOMAPF is second only to the RSS-based strategy. Figure 8(b) shows the cumulative distribution of the number of handovers under each strategy. We can observe that the handover times of users under CR-MOMAPF are second only to those of MHT-based strategy and better than those of the other three strategies. As for the number of user conflicts, it can be observed from Figure 8(c) that CR-MOMAPF is better than the RSS-based strategy and worse than MCT-based strategy. Compared with MHT-based and weighted-based strategy, CR-MOMAPF does not have obvious advantage in the average number of conflicts. This is due to the fact that reducing the number of handovers can reduce the number of conflicts to a certain extent, which is known from the definition of user conflict. However, from the total number of conflicts, there are 47 conflicts in CR-MOMAPF, which is better than 57 conflicts under the MHT-based strategy and 50 conflicts under weighted-based strategy.

Subsequently, we calculate the handover delay of each strategy based on formula (14). Figure 9 shows the change of the cumulative handover delay of all users with time. The CR-MOMAPF strategy in the figure is a solution randomly selected from the Pareto-optimal solution set. We can observe that the handover delay of the CR-MOMAPF strategy is second only to the MHT-based strategy. This is because the latter has the least number of handovers. Then, for each of these handover strategies, we count the average delay of each handover. The average handover delay is 27.68 ms for the MCT-based strategy, 25.94 ms for the weighted-based strategy, 19.87 ms for the MHT-based strategy, and 19.53 ms for the RSS-based strategy. The average handover delay of CR-MOMAPF is the best, which is 17.96 ms.

Without loss of generality, we count the performance of all solutions in the Pareto-optimal solution set and compare them with the other four strategies. We find that the cumulative handover delay of all solutions in the solution set is second only to the MHT-based strategy. Moreover, 89% of the solutions in the Pareto-optimal solution set (i.e., 381 solutions) have the lowest average handover delay. The

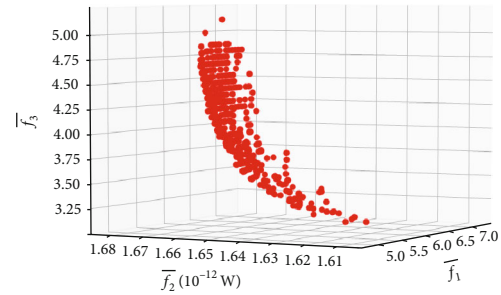

FIGURE 7: The Pareto front of the scenario with $N = 15$.

handover efficiency is improved by up to 28.31% compared with the RSS-based strategy, 29.54% compared with the MHT-based strategy, 49.41% compared with the MCT-based strategy, and 46.03% compared with the weighted-based strategy.

Finally, we compare the handover success rate under different strategies, and the results are shown in Figure 10. We can see that the solution randomly selected from the Pareto-optimal set of CR-MOMAPF has the highest handover success rate. To avoid accidents, we calculate the handover success rate of all solutions in the Pareto-optimal solution set. It is found that the lowest handover success rate is 98.76%, and the highest handover success rate is 100%. This is due to the fact that the three optimization objectives of our proposed algorithm improve the users' signal quality, reduce the number of handovers, and make the users choose the lightly loaded satellites for handover as much as possible.

In summary, our algorithm can comprehensively optimize three objectives, which further optimize the handover delay and handover success rate. Compared with the other four strategies, most of the solutions in the Pareto-optimal solution set have the best performances. The decision maker can select the appropriate handover strategy from the Pareto-optimal solution set according to the user classification.

4.5. Comprehensive Performance with Different Strategies. In this simulation, we design an index to evaluate the comprehensive performance of a solution. We firstly calculate the extremum of these three performance indexes in this problem. Then, we exploit min-max normalization to normalize the three indexes of a solution and sum them to get the evaluation index EI of the solution. EI is given by

$$\mathrm{EI} = -p_{\mathrm{normal}} + h_{\mathrm{normal}} + c_{\mathrm{normal}}, \tag{19}$$

where p_{normal}, h_{normal}, and c_{normal} are the normalized values of the received signal strength, handover times, and the number of conflicts of a solution. It can be known that the smaller the EI value of the solution, the better the comprehensive performance of the solution. In this way, we compare the solutions obtained by each handover strategy.

Based on the cities in Table 3, we select three groups of users for this simulation. The first group is the top 5 cities ($N = 5$), the second group is the top 10 cities ($N = 10$), and the third group is all 15 cities ($N = 15$). The Pareto front

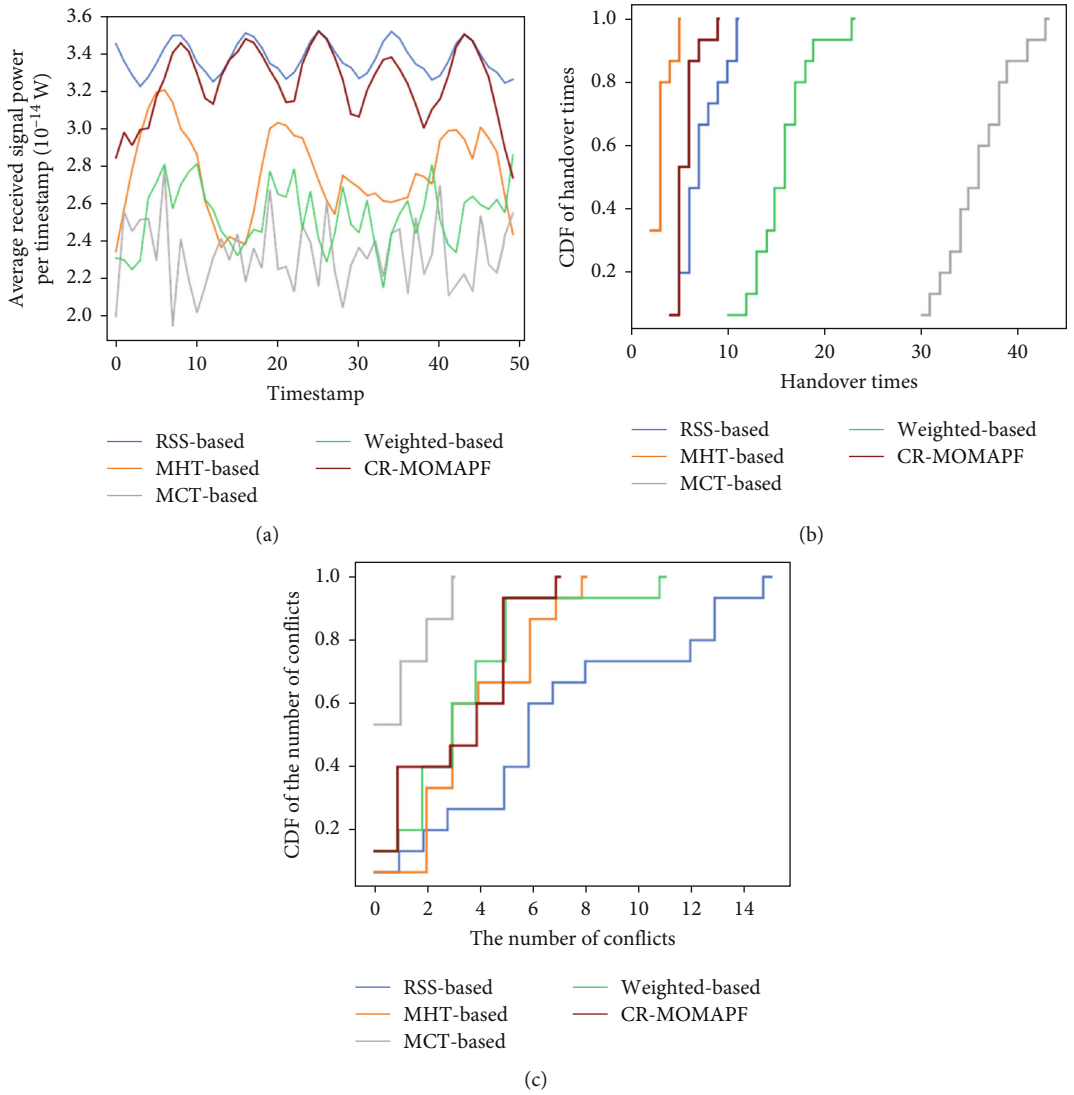

Figure 8: Performance of users with different handover strategies: (a) received signal strength; (b) handover times; (c) conflict times.

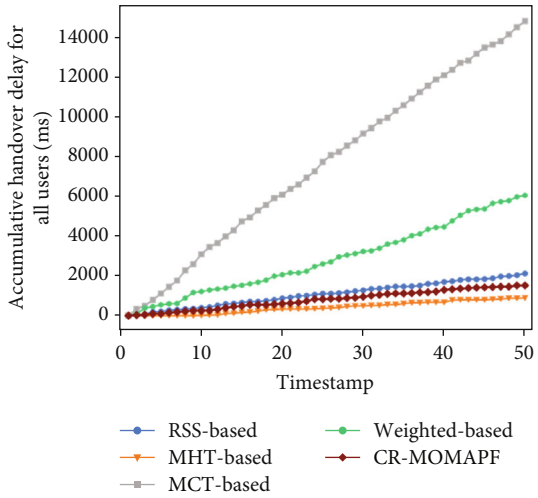

Figure 9: Comparison of accumulative handover delay for five different handover strategies.

obtained in these three scenarios is shown in Figures 6(b), 7, and 11, respectively. Eight solutions in each scenario are randomly selected from their Pareto-optimal solution sets and then presented in Table 5. As is shown in Figure 12, in the three scenarios, the comprehensive performance of randomly selected solutions in the Pareto-optimal solution sets obtained by CR-MOMAPF is the best. MCT-based strategy produces too many handovers to reduce the number of conflicts, resulting in the worst comprehensive performance. Subsequently, to avoid contingency, we calculate the EI values of all solutions in the Pareto front. The results show that in the scenarios of $N = 5$, $N = 10$, and $N = 15$, the solutions with the best comprehensive performance account for 62.5%, 87.83%, and 97.89%, respectively. The remaining solutions have the second best comprehensive performance. This means that there is a great possibility that selecting a solution from the Pareto-optimal solution set will have the best comprehensive performance.

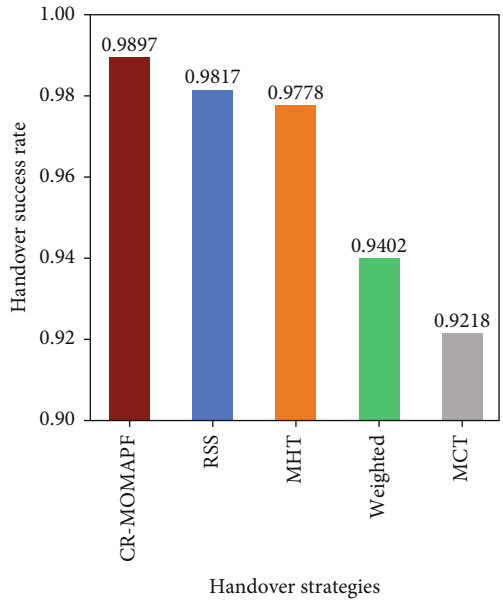

Figure 10: Comparison of handover success rate for five different handover strategies.

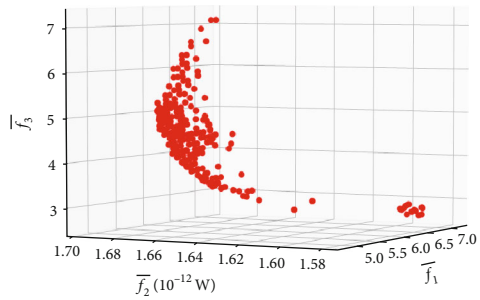

Figure 11: The Pareto front of the scenario with $N = 10$.

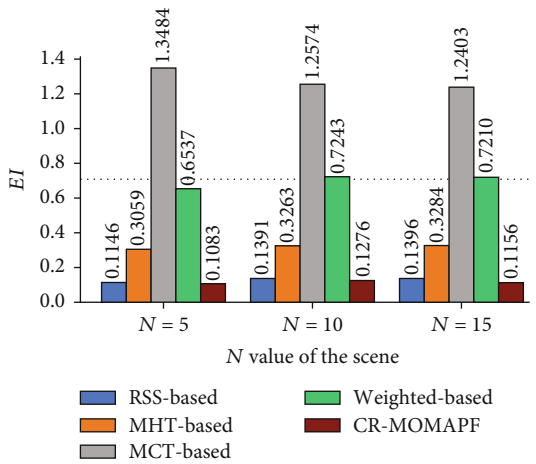

Figure 12: EI values of solutions under different strategies.

5. Conclusions

(1) A multiobjective multiagent optimization algorithm is proposed for solving the handover problem that is transformed into a path finding problem, and the transformation is implemented by the proposed multiple directed graph model. We conducted our experiments using the Starlink constellation and some terrestrial cities as scenarios

(2) The experimental results show that the algorithm finds a set of Pareto-optimal solutions for the users in the scenario. It is also shown that the average number of user conflicts in a multiuser scenario is related to the density of users. Additionally, the increase in the number of users may not lead to an increase in the number of conflicts. The number of handover and the average received signal strength are related to the location of users, but not to the density of users. Compared with other strategies, this strategy has advantages in terms of the number of solutions and the quality of performance

(3) In the future, we will study the handover strategy for multiple users with high-speed mobility and the point of incorporating handover strategy into handover protocols

Data Availability

The data used to support the findings of this study are available from the corresponding author upon request.

Conflicts of Interest

The authors declare that there is no conflict of interest regarding the publication of this paper.

Acknowledgments

This work was supported by the 173 Key Project of China (grant number 2019-JCJQ-ZD-342-00).

References

[1] C.-Q. Dai, S. Li, J. Wu, and Q. Chen, "Distributed user association with grouping in satellite–terrestrial integrated networks," *IEEE Internet of Things Journal*, vol. 9, no. 12, pp. 10244–10256, 2021.

[2] C.-Q. Dai, J. Luo, S. Fu, J. Wu, and Q. Chen, "Dynamic user association for resilient backhauling in satellite–terrestrial integrated networks," *IEEE Systems Journal*, vol. 14, no. 4, pp. 5025–5036, 2020.

[3] Y. Shi, J. Wu, L. Liu, D. Lan, and A. Taherkordi, "Energy-aware relay optimization and power allocation in multiple unmanned aerial vehicles aided satellite-aerial-terrestrial networks," *IEEE Systems Journal*, vol. 16, no. 4, pp. 5293–5304, 2022.

[4] C.-Q. Dai, Q. Yang, J. Wu, and Q. Chen, "Intelligent gateway placement in satellite-terrestrial integrated network," in *IEEE INFOCOM 2021 - IEEE Conference on Computer*

Communications Workshops (INFOCOM WKSHPS), pp. 1–6, Vancouver, BC, Canada, May 2021.

[5] Z. Lin, M. Lin, J.-B. Wang, T. De Cola, and J. Wang, "Joint beamforming and power allocation for satellite-terrestrial integrated networks with non-orthogonal multiple access," *IEEE Journal of Selected Topics in Signal Processing*, vol. 13, no. 3, pp. 657–670, 2019.

[6] Z. Lin, H. Niu, K. An et al., "Refracting RIS-aided hybrid satellite-terrestrial relay networks: Joint beamforming design and optimization," *IEEE Transactions on Aerospace and Electronic Systems*, vol. 58, no. 4, pp. 3717–3724, 2022.

[7] Z. Lin, K. An, H. Niu et al., "SLNR-based secure energy efficient beamforming in multibeam satellite systems," *IEEE Transactions on Aerospace and Electronic Systems*, pp. 1–4, 2022.

[8] K. An, M. Lin, J. Ouyang, and W.-P. Zhu, "Secure transmission in cognitive satellite terrestrial networks," *IEEE Journal on Selected Areas in Communications*, vol. 34, no. 11, pp. 3025–3037, 2016.

[9] S. Kassing, D. Bhattacherjee, A. B. Aguas, J. E. Saethre, and A. Singla, "Exploring the "Internet from space" with Hypatia," in *in Proceedings of the ACM Internet Measurement Conference*, pp. 214–229, New York, NY, USA, 2020.

[10] 3GPP, "Solutions for NR to support non-terrestrial networks (NTN)," in *3rd Generation Partnership Project (3GPP), TR 38.821, version 16.0.0*, 2020, https://www.3gpp.org/ftp/Specs/archive/38_series/38.821/.

[11] P. K. Chowdhury, M. Atiquzzaman, and W. Ivancic, "Handover schemes in satellite networks: state-of-the-art and future research directions," *IEEE Communications Surveys & Tutorials*, vol. 8, no. 4, pp. 2–14, 2006.

[12] C.-Q. Dai, J. Xu, J. Wu, and Q. Chen, "Multi-objective intelligent handover in satellite-terrestrial integrated networks," in *2022 IEEE International Conference on Communications Workshops (ICC Workshops)*, pp. 367–372, Seoul, South Korea, May 2022.

[13] Y. Liu, L. Feng, L. Wu et al., "Joint optimization based satellite handover strategy for low earth orbit satellite networks," *IET Communications*, vol. 15, no. 12, pp. 1576–1585, 2021.

[14] Y. H. Lei, L. F. Cao, and M. Da Han, "A handover strategy based on user dynamic preference for LEO satellite," in *2021 7th International Conference on Computer and Communications (ICCC)*, pp. 1925–1929, Chengdu, China, 2021.

[15] Y. Cao, S.-Y. Lien, and Y.-C. Liang, "Deep reinforcement learning for multi-user access control in non-terrestrial networks," *IEEE Transactions on Communications*, vol. 69, no. 3, pp. 1605–1619, 2020.

[16] S. He, T. Wang, and S. Wang, "Load-aware satellite handover strategy based on multi-agent reinforcement learning," in *GLOBECOM 2020 - 2020 IEEE Global Communications Conference*, pp. 1–6, Taipei, Taiwan, 2020.

[17] T. Leng, Y. Xu, G. Cui, and W. Wang, "Caching-aware intelligent handover strategy for LEO satellite networks," *Remote Sensing*, vol. 13, no. 11, p. 2230, 2021.

[18] H. Xu, D. Li, M. Liu, G. Han, W. Huang, and C. Xu, "QoE-driven intelligent handover for user-centric mobile satellite networks," *IEEE Transactions on Vehicular Technology*, vol. 69, no. 9, pp. 10127–10139, 2020.

[19] J. Wang, W. Mu, Y. Liu, L. Guo, S. Zhang, and G. Gui, "Deep reinforcement learning-based satellite handover scheme for satellite communications," in *2021 13th International Conference on Wireless Communications and Signal Processing (WCSP)*, pp. 1–6, Changsha, China, 2021.

[20] Y. Wu, G. Hu, F. Jin, and J. Zu, "A satellite handover strategy based on the potential game in LEO satellite networks," *IEEE Access*, vol. 7, pp. 133641–133652, 2019.

[21] L. Feng, Y. Liu, L. Wu, Z. Zhang, and J. Dang, "A satellite handover strategy based on MIMO technology in LEO satellite networks," *IEEE Communications Letters*, vol. 24, no. 7, pp. 1505–1509, 2020.

[22] Z. Wu, F. Jin, J. Luo, Y. Fu, J. Shan, and G. Hu, "A graph-based satellite handover framework for LEO satellite communication networks," *IEEE Communications Letters*, vol. 20, no. 8, pp. 1547–1550, 2016.

[23] X. Hu, H. Song, S. Liu, and W. Wang, "Velocity-aware handover prediction in LEO satellite communication networks," *International Journal of Satellite Communications and Networking*, vol. 36, no. 6, pp. 451–459, 2018.

[24] C.-Q. Dai, Y. Liu, S. Fu, J. Wu, and Q. Chen, "Dynamic handover in satellite-terrestrial integrated networks," in *2019 IEEE Globecom Workshops (GC Wkshps)*, pp. 1–6, Waikoloa, HI, 2019.

[25] K. Deb, A. Pratap, S. Agarwal, and T. Meyarivan, "A fast and elitist multiobjective genetic algorithm: NSGA-II," *IEEE Transactions on Evolutionary Computation*, vol. 6, no. 2, pp. 182–197, 2002.

[26] K. Deb and H. Jain, "An evolutionary many-objective optimization algorithm using reference-point-based nondominated sorting approach, part I: solving problems with box constraints," *IEEE Transactions on Evolutionary Computation*, vol. 18, no. 4, pp. 577–601, 2014.

[27] B. Yang, Y. Wu, X. Chu, and G. Song, "Seamless handover in software-defined satellite networking," *IEEE Communications Letters*, vol. 20, no. 9, pp. 1768–1771, 2016.

[28] C. Loo, "A statistical model for a land mobile satellite link," *IEEE Transactions on Vehicular Technology*, vol. 34, no. 3, pp. 122–127, 1985.

[29] L. You, K. X. Li, J. Wang, X. Gao, X. G. Xia, and B. Ottersten, "Massive MIMO transmission for LEO satellite communications," *IEEE Journal on Selected Areas in Communications*, vol. 38, no. 8, pp. 1851–1865, 2020.

[30] X. Ding, Z. Zhang, and D. Liu, "Low-delay secure handover for space-air-ground integrated networks," in *IEEE 31st Annual International Symposium on Personal, Indoor and Mobile Radio Communications*, pp. 1–6, London, UK, 2020.

[31] P. Zhou, Y. Liu, L. Guo, N. Lu, J. Wu, and H. Jiang, "Handoff of satellite network for high-speed mobile terminals based on edge computing," in *2021 8th IEEE International Conference on Cyber Security and Cloud Computing (CSCloud)/2021 7th IEEE International Conference on Edge Computing and Scalable Cloud (EdgeCom)*, pp. 167–175, Washington, USA, 2021.

[32] T. Standley, "Finding optimal solutions to cooperative pathfinding problems," in *Proceedings of the AAAI Conference on Artificial Intelligence*, pp. 173–178, Atlanta, GA, 2010.

[33] G. Sharon, R. Stern, A. Felner, and N. R. Sturtevant, "Conflict-based search for optimal multi-agent pathfinding," *Artificial Intelligence*, vol. 219, pp. 40–66, 2015.

[34] Z. Ren, S. Rathinam, and H. Choset, "Multi-objective conflict-based search for multi-agent path finding," in *2021 IEEE International Conference on Robotics and Automation (ICRA)*, pp. 8786–8791, Xian, Peoples R China, May 2021.

[35] Z. Ren, S. Rathinam, and H. Choset, "Subdimensional expansion for multi-objective multi-agent path finding," *IEEE Robotics and Automation Letters*, vol. 6, no. 4, pp. 7153–7160, 2021.

[36] J. Weise, S. Mai, H. Zille, and S. Mostaghim, "On the scalable multi-objective multi-agent pathfinding problem," in *2020 IEEE Congress on Evolutionary Computation (CEC)*, pp. 1–8, Glasgow, UK, 2020.

[37] D. Bhattacherjee and A. Singla, "Network topology design at 27,000 km/hour," in *Proceedings of the 15th International Conference on Emerging Networking Experiments And Technologies*, pp. 341–354, Orlando, LA, 2019.

[38] CesiumGS, "Cesium," 2022, https://github.com/CesiumGS/cesium.

[39] L. Lin and M. Gen, "Priority-based genetic algorithm for shortest path routing problem in OSPF," in *Intelligent and Evolutionary Systems. Studies in Computational Intelligence*, vol. 187, Springer, Berlin, Heidelberg, 2004.

[40] J. M. Bogoya, A. Vargas, and O. Schutze, "The averaged Hausdorff distances in multi-objective optimization: a review," *Mathematics*, vol. 7, no. 10, p. 894, 2019.

[41] H. Briantoro, N. Funabiki, M. Kuribayashi et al., "Transmission power optimization of concurrently communicating two access points in wireless local area network," *International Journal of Mobile Computing and Multimedia Communications*, vol. 11, no. 4, pp. 1–25, 2020.

[42] J. Jazzbin, "Geatpy: the genetic and evolutionary algorithm toolbox with high performance in Python," 2020, https://github.com/geatpy-dev/geatpy.

[43] J. Miao, P. Wang, H. Yin, N. Chen, and X. Wang, "A multi-attribute decision handover scheme for LEO mobile satellite networks," in *2019 IEEE 5th International Conference on Computer and Communications (ICCC)*, pp. 938–942, Chengdu, China, 2019.